Soot and charcoal as reservoirs of extracellular DNA

S. Jelavić,[a,b*] L.G. Thygesen,[c] V. Magnin,[b] N. Findling,[b] S. Müller,[d] V. Meklesh,[e] K.K. Sand[a]

[a]Centre for Geogenetics, GLOBE Institute, University of Copenhagen, Øster Voldgade 5–7, 1350 Copenhagen, Denmark.

[b]Université Grenoble Alpes, Université Savoie Mont Blanc, CNRS, IRD, Université Gustave Eiffel, ISTerre, F-38000 Grenoble, France.

[c]University of Copenhagen, Department of Geoscience and Natural Resource Management, Rolighedsvej 23, 1958 Frederiksberg C, Denmark.

[d]University of Copenhagen, Department of Geosciences and Natural Resource Management, Øster Voldgade 10, 1350 Copenhagen K, Copenhagen, Denmark.

[e]Centre for Environmental and Climate Science, Lund University, Sölvegatan 37, 223 62 Lund, Sweden.

*corresponding author: stanislav.jelavic@univ-grenoble-alpes.fr

ABSTRACT

The vast potential of using sediment adsorbed DNA as a window to past and present biodiversity rely on the ability of solid surfaces to adsorb environmental DNA. However, a comprehensive insight into DNA adsorption at surfaces in general is lacking. Soot and charcoal are carbonaceous materials widespread in the environment where they readily can come in contact with extracellular DNA shed from organisms. Using batch adsorption, we measured DNA adsorption capacity at soot and charcoal as a function of solution composition, time and DNA length. We observed that the adsorption capacity for DNA is highest at low pH, that it increases with solution concentration and cation valency and that the activation energy for DNA adsorption at both soot and charcoal is ~50 kJmol^{-1}, suggesting strong binding. We demonstrate how the interaction between DNA and soot and charcoal partly occurs via terminal base pairs, suggesting that, besides electrostatic forces, hydrophobic interactions play an important role in binding. The large adsorption capacities and strong binding of DNA to soot and charcoal are features important for eDNA research and provide a motivation for use of carbonaceous materials from, e.g. anthropogenic pollution or wildfire as sources of biodiversity information.

INTRODUCTION

Environmental DNA (eDNA) is genetic information shed from living or deceased organisms into their surroundings. Free extracellular eDNA degrades in matter of days but when adsorbed to minerals in sediments, it can be preserved for thousands of years.[1,2] The adsorptive protection provided by minerals is likely a result of disrupted molecular recognition of adsorbed DNA by enzymes[3,4] and the inactivation of enzymes by adsorption to the same surfaces.[5] Once adsorbed, the eDNA can be transported across time and space following sedimentary processes. Consequently, mineral stored eDNA is a unique resource of information relevant for estimating past and present biodiversity,[6] monitoring of invasive and endangered species[7] and for reconstruction of paleoenvironments.[8] Given that eDNA can be extracted from water, sediments[9] and air,[10,11] the contribution of common non-

mineral environmental surfaces such as carbonaceous materials (CM) to the environmental reservoir of DNA is unclear.

CMs are produced anthropogenically and naturally by burning fossil fuels and vegetation. CMs are ubiquitous in soils and, because of their low density and small size, they are easily transported by air to aqueous environments including freshwater and marine sediments.[12] The abundance, easy transportation and widespread occurrence renders soot and charcoal as promising reservoirs of eDNA. Incomplete combustion of fossil fuels produces soot while burning of vegetation produces both charcoal by pyrolysis and soot by combustion and condensation of gases within fire. There is a great variability in structure and composition of soot and charcoal depending on their source materials and temperature of formation.[12,13] In general, both can be envisaged as polycyclic aromatic materials built from agglomerates of ordered graphitic domains consisting of sp^2-hybridised carbon and domains that deviate from a perfect graphitic structure with an increased incorporation of oxygen and hydrogen.[14–16] An important difference is that the graphitic domains in soot can occur at relatively lower temperatures[13] than charcoal[17] and that charcoal can contain a core of unburnt biomass.

Knowledge of the binding between the DNA and CMs is important for understanding the adsorption under various environmental conditions. Extracellular eDNA is principally double stranded DNA (dsDNA) since this form is more resistant to degradation than single stranded DNA.[18–21] Studies of the interaction between dsDNA and materials compositionally and structurally similar to soot and charcoal such as graphene, graphene oxide (GO) and reduced graphene oxide (rGO) have already provided insight into the eDNA binding at CMs.[22–24] Molecular dynamics simulation suggested that, at oxygen-lacking CM's such as graphene, dsDNA binds to surface via the terminal base pairs through π–π stacking.[25] dsDNA can bind either using only one termination, with the helix axis perpendicular to the graphene surface ("standing up"), or with both terminations forming a horseshoe shape, with the axis mostly parallel to the surface except close to terminations where base pairs are severely deformed. From studies of oxygen-containing CM's such as GO and rGO, we know that dsDNA can bind either electrostatically via the negatively phosphate backbone (helix axis parallel to adsorbent surface - "lying down") or by π–π interaction and hydrogen bonding via the base pairs at the end of DNA,[26–28] as with graphene. In the absence of electrolytes that reduce electrostatic repulsion between negatively charged GO or rGO and negatively charged phosphate backbone, bulk adsorption studies suggest that hydrophobic forces dominate the interaction with DNA.[29] However, in the presence of electrolytes, electrostatic interaction becomes more important evidenced by increasing DNA adsorption capacity as the ionic strength increases[29,30] or as pH decreases.[29] The distribution of oxygen functional groups in GO and rGO is highly heterogeneous,[31,32] *i.e.*, they contain areas that are rich and areas that are poor in functional groups. The interaction between these surfaces and the phosphate backbone likely takes places at the areas rich in hydrophilic functional groups. In contrast, the π – π stacking takes place at areas poor in oxygen functional groups (graphene-like). Combined, these studies suggest that the ratio of hydrophilic and hydrophobic areas in carbonaceous materials determines their overall interaction with dsDNA, with hydrophobic interactions becoming dominant in materials rich in graphene-like surfaces. However, graphene-like materials are rare in the environment and it is unclear to which extent our current understanding of DNA interactions with carbonaceous materials is applicable to environmentally common surfaces such as soot and charcoal.

We determined the composition of soot and charcoal using Scanning Electron Microscopy (SEM), X-ray Diffraction (XRD) and X-ray Photoelectron Spectroscopy (XPS), the structure using Raman Spectroscopy, and the surface properties using water vapour adsorption, mass titration and electrokinetic measurements. To elucidate how structure, composition and surface properties influence DNA adsorption at soot and charcoal, we measured the adsorption capacity for DNA as a

function of pH, ionic strength, solution composition, time and DNA length. We used isotherm modelling to quantify differences in isotherm shapes. By evaluating how the surface properties of soot and charcoal influence the adsorption of DNA as a function of solution composition, we infer a likely adsorption mechanism. We propose that, besides electrostatic forces, hydrophobic interactions play an important role in adsorption of DNA to soot and charcoal. This information can be used for improving protocols of eDNA extraction from environmental matrices where soot and charcoal are abundant such as urban and wildfire aerosol, and topsoil. This is important because DNA adsorbed at soot and charcoal could hold (paleo)biodiversity information that is not available through routine eDNA extraction and analysis. Advancing our understanding of interactions between DNA and environmental surfaces will provide an important contribution to understanding of eDNA reservoirs in the environment.

MATERIALS AND METHODS

Material characterisation

We purchased carbon soot nanopowder (NANOSHEL, >98.9%, CAS: 7440-44-0), further called soot, and activated charcoal (DARCO, Sigma Aldrich), further called charcoal. We used XRD to identify major and minor contaminants. We collected diffractograms between 5-90 °2Θ using a Bruker D8 diffractometer equipped with Cu K_α radiation (40 kV, 40 mA; λ ~ 1.543 Å). We used step size of 0.04 °2Θ, time per step of 6 s and spun the sample at 20 rpm with 0.3° divergence and antiscatter slit and 2.3° Soller slits on both incident and diffracted beams.

We identified trace phases using SEM by fixing powders on a double-sided carbon tape and sputter coated them with ~1 nm of Au. Images and energy-dispersive spectra were obtained using Vega-3 Tescan microscope. Both images and spectra were collected with a beam operated at 20 kV.

The surface elemental composition was determined using XPS. We used double-sided sticky tape to fix the samples. Wide and high-resolution spectra were collected using PHI X-tool instrument (Physical Electronics Inc., Chanhassen, MN, USA) (excitation energy *hv* = 1486.7 eV, tension voltage 18 kV, emission power 52 W) with a spot size of 205 μm^2. The photoelectrons were collected at 45° take-off angle using a pass energy of 280 eV with a step of 0.25 eV. The spectra calibration was done by assigning the C1s peak to 284.8 eV.

To estimate the structural disorder of soot and charcoal, we used Raman spectroscopy. We spread the powders on Al-foil and acquired spectra with a 532 nm Ar-laser operated at 100% effect (approximately 60 mW before the objective) using a WITec alpha 300R confocal Raman microscope (WITec GmbH). The spectral resolution of the spectrometer (UHTS300 spectrometer VIS) was 3.8 cm^{-1}. Each spectrum was obtained as the mean of 100, 0.1 s scans. We removed signal from cosmic rays by median filtering and corrected the background by an asymmetric least square algorithm. The spectra were then Savitzky-Golay smoothened to minimise the noise. Each sample was analysed in at least triplicates. We used a relative intensities of G (~1560 cm^{-1}), D1 (~1350 cm^{-1}) and D2 (~1600 cm^{-1}) bands to estimate the fraction of a ordered graphitic component, *i.e.* the structural order of soot and charcoal.[33–36] In addition, we calculated *R2* parameter to estimate the disorder in soot and charcoal:[37]

$$R2 = \frac{I\ (D_1)}{I\ (D_1) + I\ (G) + I\ (D_2)}, \qquad \text{Eq 1}$$

where *I* represents an integrated area under the band.

To estimate point of zero charge (PZC), we used mass titration.[38,39] We prepared three solutions with different initial pH (pH_0 ~ 11, ~ 6 and ~ 3). 15 ml vials contained 5 ml of either 100 mM $NaNO_3$ (ACS reagent, ≥99.0%, Fluka) to estimate PZC in an inert background electrolyte, and 5 and 1 mM $CaCl_2$ (hexahydrate, ACS reagent, ≥99%, Sigma Aldrich) to estimate the effect of divalent cations on PZC. The pH was adjusted using 0.1 M HNO_3 and 0.1 M NaOH for $NaNO_3$ solution, and 0.1 M HCl (all Fixanal, Fluka analytical) and 0.1 M NaOH for $CaCl_2$ solutions. We then added soot or charcoal powder to reach a target weight of a solid (wt.%), rotated the vials for ~2 h at 30 rpm for suspension to equilibrate and then measured the suspension pH before adding another batch of powder.

For the electrokinetic measurements, we used a suspension of 1 $mgml^{-1}$ of soot and charcoal prepared with 1 and 5 mM $CaCl_2$. We titrated a 10 ml suspension with 0.05 mM HCL in 0.5 µL steps and simultaneously recorded pH and ζ potential using a Stabino instrument (Colloid Metrics GmbH, Germany). The instrument contains a PTFE chamber with an oscillating piston that is slightly negatively charged. A particle solution is added and van der Waal forces cause particle adsorption at the wall, yet a fraction is immobilized. Due to the movement of the piston a mobile cloud of double layer is formed and set in motion. Such oscillating ion cloud generates a voltage, which is captured by two separate electrodes, defining the streaming potential of the solution, which is proportional to the zeta potential of the particles. The Stabino streaming potential method can measure across a large particle size range (0.3nm-300µm) and particle concentrations up to 40 vol.%. Moreover, optical properties of the liquid are not relevant for its measurement, unlike electrophoresis method, which may be challenging when working with soot and charcoal.

To estimate a hydrophobic character of soot and charcoal, we volumetrically collected water vapor isotherms at 25 °C using a BELSORP-MAX instrument from BEL Japan. Prior, powders were outgassed at 150 °C for 24 h at a residual pressure of 10^{-5} – 10^{-4} Pa.

Batch adsorption experiments

Materials. We used low molecular weight salmon sperm double stranded DNA (lyophilised powder, Sigma Aldrich) with a size of ~30 base pairs (bp) because it is easily accessible in large amounts and concentrations required for obtaining reliable adsorption isotherms. Since 30 bp is on the shorter end of extracted environmental (ancient) DNA, we looked into the influence of DNA length on adsorption capacity of soot and charcoal by comparing it to adsorption of double stranded DNA salmon sperm solution (UltraPure, 10 $mgml^{-1}$, ThermoFischer Scientific) with the size of ≤2000 bp. We used DNA LoBind tubes (Eppendorf) and DNase/RNase-free water (molecular biology water, LONZA, AccuGene) for preparation of all solutions and suspensions. The pH of stocks and suspensions was adjusted with 0.1 M HCl and 0.1 M NaOH and measured with 913 Metrohm metre calibrated on a daily basis (precision ± 0.1 unit). We did not use pH buffers as they are known to modify DNA adsorption capacity.[40] We prepared 1 mM and 100 mM electrolyte stocks of NaCl (ACS reagent, ≥99%, anhydrous, Sigma Aldrich) and $CaCl_2$, and soot and charcoal stock suspensions at the concentration of 50 $mgml^{-1}$. Immediately prior to an experiment, we prepared 1 $mgml^{-1}$ DNA stock (30 bp) by dissolving lyophilised powder in electrolyte suspension, shaked it for 15 min at 20 °C at 300 rpm on an orbital shaker and adjusted the pH.

Batch equilibrium adsorption. For adsorption experiments, we mixed 10 μl of a stock suspension (soot or charcoal) with the predetermined volume of electrolyte solution or pure water in 2 ml tube and ultrasonicated it for 10 min to break aggregates. We then added DNA stock to a final volume of 1 ml, vortexed the sample for a couple of seconds and placed it on a revolver rotator (18 rpm). The final mass concentration of suspensions was 0.5 – 0.6 μgml^{-1}. To obtain reliable isotherms for adsorption modelling, we prepared 5-8 different DNA concentrations between 10 – 800 μgml^{-1}, in triplicates. After

6 h of equilibration at room temperature, we centrifuged the tubes for 3 min at 5000 rpm and separated top 200 µl of the supernatant for UV spectrometry (Biophotometer, Eppendorf) using microcuvettes (BRAND). To account for turbidity, we determined the DNA concentration by subtracting the absorbance of the supernatant at 320 nm from the absorbance at 260 nm. To account for various instrumental uncertainties, the subtracted absorbance was read from a DNA calibration curve calculated on an everyday basis from freshly prepared DNA standards.

When we looked at the influence of pH, solvents (ethanol, BioReagents, absolute, Fisher Scientific; isopropanol, Bioreagent, ≥99%, Sigma Aldrich), and phosphates (Na-polyphosphate, ≥68% P_2O_5 basis, EMPLURA, Supelco; Na-metaphosphate, 96%, Sigma Aldrich) on adsorption, we followed the same protocol as for isotherms, except that the stock was diluted to only one initial DNA concentration, 50 $mgml^{-1}$.

Kinetic experiments. The kinetic experiments were done using initial DNA concentration of 50 $mgml^{-1}$, in 100 mM NaCl solution and at three temperatures: 283, 293 and 303 K (Eppendorf ThermoMixer; precision ±0.2 K). To have enough suspension to sample over the course of the experiment, we upscaled the quantities and used 15 ml instead of 2 ml tubes as was done in adsorption studies. We equilibrated the suspension and the DNA solution separately for 2 h at desired temperature before mixing them together to minimise temperature fluctuations over the course of experiment. At various time intervals (3 min – 29 h), 200 µl of suspension were extracted and centrifuged for 3 min at 5000 rpm and the supernatant was kept for UV measurement. The sampling time reported includes centrifugation time, i.e. the sampling time of 6 min means that the sample was equilibrated for 3 minutes in thermomixer and then centrifuged for 3 minutes.

Calculation of adsorption capacities. The equilibrium adsorption capacity of DNA (q_{eq}, μgmg^{-1}) was determined as a function of equilibrium DNA concentration in solution ($c_{eq,}$ μgml^{-1}) by taking:

$$q_{eq} = \frac{c_i - c_{eq}}{\gamma}, \qquad \text{Eq 2}$$

where c_i (μgml^{-1}) represents the initial concentration of DNA and γ represents the mass concentration of soot or charcoal ($mgml^{-1}$). For kinetic experiments, we determined the adsorption capacity q_t ($mgml^{-1}$) at time t (min):

$$q_t = c_i - c_t, \qquad \text{Eq 3}$$

where c_t (μgml^{-1}) represents DNA concentration measured in the supernatant at time t. Throughout the paper, we refer to a plot of q_{eq} vs. c_{eq} as an adsorption isotherm and to a plot of q_t vs. t as kinetic data.

Modelling of equilibrium adsorption and kinetic data. We fit the adsorption isotherms using equations that model monolayer and multilayer adsorption (but acknowledge that such modelling alone does not reveal how adsorption takes place in reality), and the kinetic data using equations that model surface and diffusion controlled processes (Table S1.). We applied nonlinear least squares regression to fit data to models. We chose the mathematically best fitting model by comparing their reduced chi-squared parameter of fits, χ^2_ν, *i.e.* the χ^2_ν closest to 1 was considered the best. If the best fit resulted in standard errors that were larger than the fitting parameters, the fit with χ^2_ν that was next in line but with standard errors smaller than the fitting parameters was considered more appropriate, i.e., matching the form of curve better.

RESULTS AND DISCUSSION

Composition and properties of soot and charcoal

Phase and elemental composition. Both soot and charcoal are largely composed of poorly ordered graphite-like carbon material as evidenced by the presence of broad diffraction peaks between 15 - 30 °2Θ, corresponding to graphite (001) reflection, and 40 - 50 °2Θ, corresponding to a combination of graphite (100) and (101) reflections (Fig. 1A). In addition, soot contains quartz (SiO_2) as a minor impurity identified by XRD and trace amounts of titanite ($CaTiSiO_5$; Fig. S1a) and chlorapatite ($Ca_5(PO_4)_3Cl$; Fig. S1b) identified by EDX spectroscopy. Charcoal contains minor quartz and Na-rich plagioclase ($(Na,Ca)(Al,Si)_4O_8$) (Fig. 1A), and trace amounts of likely a Ca-Mg carbonate (either Mg-calcite ($CaCO_3$) or dolomite ($CaMg(CO_3)_2$; Fig. S2b), an Fe-O phase (Fig. S2c) and TiO_2 phase (Fig. S2d). XPS showed that the surface of soot contained 90.9 At.% of C and 9.1 At.% of O with trace amounts of Si, N and S while charcoal contained 93.0 At.% of C and 7.0 At.% of O with trace amounts of N, Si and Al (Figure 1B). Since quartz and plagioclase contain Si and Al, the small surface concentration of these elements confirm that the contribution of mineral impurities to reactions at soot and charcoal surfaces is likely negligible.

Structural (Raman) properties. We observed three bands in Raman spectra of soot and charcoal (Fig. 1C-D): D_1 (~1350 cm^{-1}), G (~1560 cm^{-1}) and D_2 (~1600 cm^{-1}) bands. The band position is comparable between soot (D_1= 1348 ± 6 cm^{-1}, G= 1567 ± 2 cm^{-1}, D_2= 1598 ± 2 cm^{-1}) (Fig. 1C) and charcoal (D_1= 1348 ± 5 cm^{-1}, G= 1563 ± 2 cm^{-1}, D_2= 1606 ± 2 cm^{-1}) (Fig. 1D). For soot, the G band is relatively more intense compared to both D_1 and D_2 than for charcoal suggesting that soot contains larger volume of an ordered graphitic component. *R2* parameter (Eq. 1) is smaller for soot (0.554 ± 0.027) compared to charcoal (0.642 ± 0.006) indicating that soot is overall more ordered and more graphite-like than charcoal.

Surface properties. In an inert electrolyte (100 mM $NaNO_3$), the PZC of soot (8.3 ± 0.1; Fig. S3a) and charcoal (9.5 ± 0.1; Fig. S3b) was comparable to previous studies on CMs that used mass titration.[41–44] In $CaCl_2$ solutions, the PZC was lower than in $NaNO_3$ for both soot (7.7 ± 0.1; Fig. 1E) and charcoal (8.3 ± 0.2; Fig. 1F) likely reflecting an increase in surface charge density in divalent electrolyte solutions as a result of cation adsorption. The IEP for both materials determined by electrokinetic measurements, however, was significantly lower: for soot, IEP in 1 mM $CaCl_2$ was ~ 3.4 and in 5 mM CaCl2 ~ 3.6 (Fig. 1G) while for charcoal it was ~ 3.0 in 1 mM $CaCl_2$ and 3.0 – 3.5 in 5 mM $CaCl_2$ (Fig. 1H). The increase of IEP with an increase in ionic strength reflects a more efficient screening of negatively charged active sites. IEP represents a pH value at which the electrokinetic potential equals zero, i.e. particle is not mobile under applied electric field, while PZC represents a pH value at which the net surface potential of all particle surfaces equals zero. Since IEP is lower than PZC, the surfaces that control the particle mobility (external surfaces) are more negatively charged than particles whose charge has little influence on mobility (internal surfaces) but can still be probed by proton adsorption, i.e. the titration experiment.[43] The difference between IEP and PZC implies a heterogeneous distribution of surface charges of both soot and charcoeal[43] and suggests that both behave as negatively charged surfaces in circumneutral solutions.

Both soot and charcoal adsorbed only 2 - 3 molecules of water at low pressures (p/p_0<0.4, Fig. 1I), a characteristic of hydrophobic surfaces.[45,46] The difference in the adsorbed water between soot and charcoal is <0.1 molecule/nm, reflecting a similar surface composition determined with XPS (Fig. 1B) and suggesting no significant difference in bulk hydrophobicity between soot and charcoal.

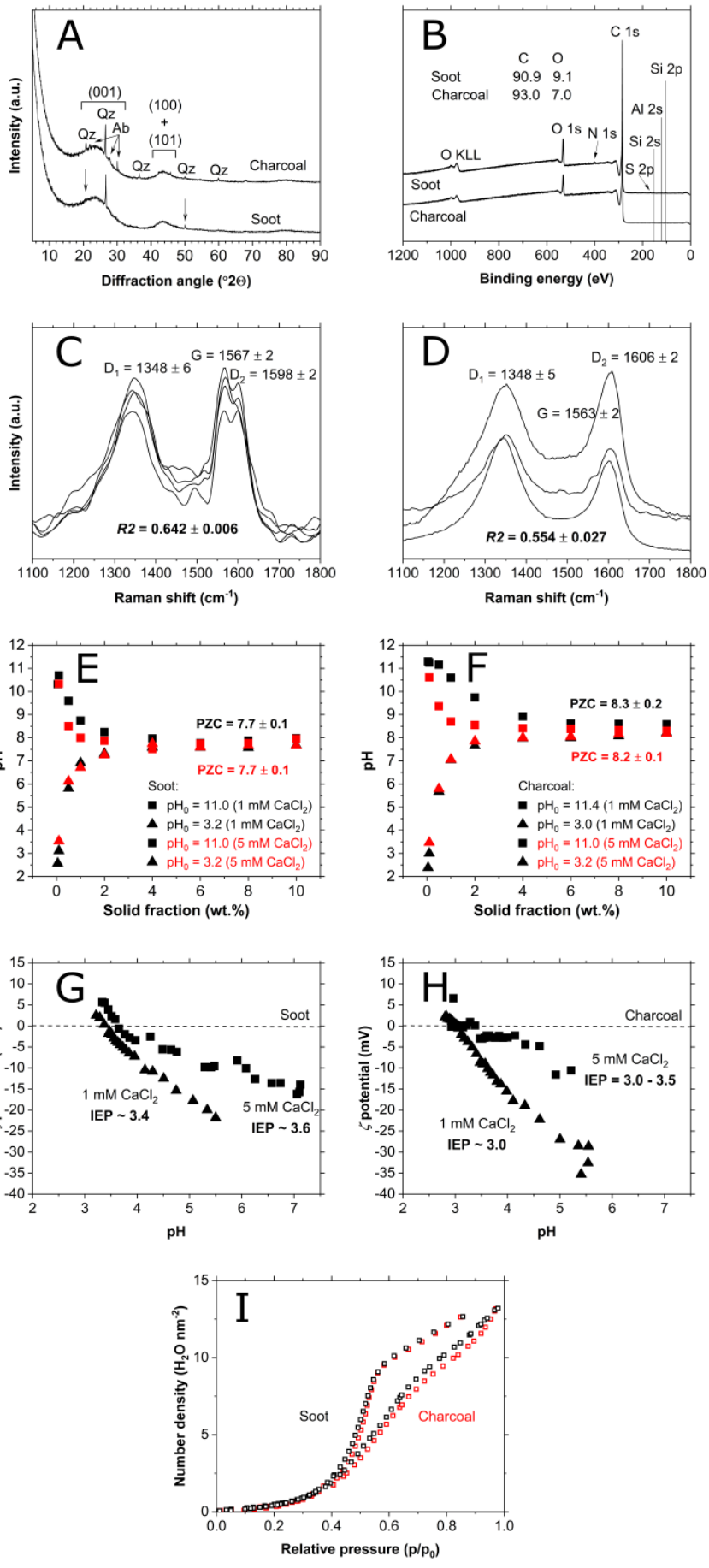
A
Intensity (a.u.)
(001)
Qz
Ab
(100)
+
(101)
Qz
Charcoal
Soot
Diffraction angle (°2Θ)
B
C 1s
Si 2p
Soot
Charcoal
C
O
90.9
9.1
93.0
7.0
Al 2s
O 1s
N 1s
Si 2s
O KLL
S 2p
Binding energy (eV)
C
D1 = 1348 ± 6
G = 1567 ± 2
D2 = 1598 ± 2
R2 = 0.642 ± 0.006
Raman shift (cm-1)
D
D1 = 1348 ± 5
D2 = 1606 ± 2
G = 1563 ± 2
R2 = 0.554 ± 0.027
E
PZC = 7.7 ± 0.1
PZC = 7.7 ± 0.1
Soot:
pH0 = 11.0 (1 mM CaCl2)
pH0 = 3.2 (1 mM CaCl2)
pH0 = 11.0 (5 mM CaCl2)
pH0 = 3.2 (5 mM CaCl2)
pH
Solid fraction (wt.%)
F
PZC = 8.3 ± 0.2
PZC = 8.2 ± 0.1
Charcoal:
pH0 = 11.4 (1 mM CaCl2)
pH0 = 3.0 (1 mM CaCl2)
pH0 = 11.0 (5 mM CaCl2)
pH0 = 3.2 (5 mM CaCl2)
G
Soot
1 mM CaCl2
IEP ~ 3.4
5 mM CaCl2
IEP ~ 3.6
ζ potential (mV)
pH
H
Charcoal
5 mM CaCl2
IEP = 3.0 - 3.5
1 mM CaCl2
IEP ~ 3.0
I
Soot
Charcoal
Number density (H2O nm-2)
Relative pressure (p/p0)

252

Figure 1. a) XRD patterns with assigned diffraction peaks from the graphite structure; Qz – quartz and Ab- albite occur as minor components. b) XPS results and quantitative analysis with assigned photoelectron peaks. c) soot and d) charcoal Raman spectra containing peak assignment and their shift. Uncertainties are reported as a range of detected shifts. Mass titration with e) soot and f) charcoal started from different initial pH values (pH_0). Electrokinetic measurements of g) soot and h) charcoal with the corresponding isoelectric points (IEP) determined as an average between neighbouring data points above and below 0 mV. h) Number of H_2O molecules per surface area is similar between soot (black) and charcoal (red) as determined from water adsorption measurements.

Adsorption

pH dependence. The equilibrium adsorption capacity (q_{eq}) of DNA at soot and charcoal decreases as pH increases (Figure 2A). The capacity is lowest between 6<pH<8 (soot=61±1 μgmg^{-1}, charcoal=72±0 μgmg^{-1}). At pH<6, the capacity increases reaching the maximum at pH=3 (soot=70±2 μgmg^{-1}, charcoal=83±2 μgmg^{-1}). Since the pK_a of the phosphoester in the backbone of DNA is ~1, and soot and charcoal behave as negatively charged particles above ~3 (Fig. 1G-H), a decrease in adsorption capacity with an increase in pH suggests that the electrostatic interaction plays a role in the interaction. One would expect that at circumneutral pH, when both DNA, and soot and charcoal are negatively charged, the adsorption would be minimal and the capacity would be close to zero. However, a significant amount of DNA is still adsorbed: at both soot and charcoal there is still ~86% of DNA of the capacity at pH=3. This cannot be due to adsorption at internal particle surfaces that are more positive than the external particle surfaces (Figure 1E-F) because the external surfaces are even more negative at circumneutral pH (<-10 mV, Fig. 1G-H) thus repelling DNA. This suggest that the electrostatics is not the only interaction governing the adsorption.

Adsorption isotherms. In all solutions and at all DNA concentrations, the adsorption capacity of charcoal was higher than that of soot (Figure 2B-C). This is even more pronounced when comparing the adsorption capacity per surface area since specific surface area of charcoal is smaller (923 m^2g^{-1}) than of soot (973 m^2g^{-1}) (Table S2). As the equilibrium solution concentration of DNA (c_{eq}) increased, q_{eq} of both soot (Figure 2B) and charcoal (Figure 2C) increased abruptly until c_{eq} ~ 100 μgmg^{-1} after which the increase is gradual. Regardless of the cation, q_{eq} was always higher at high cation concentration (100 mM–full symbols) than at low (1 mM–empty simbols), likely because of more efficient screening of electrostatic repulsion between negatively charged DNA, and soot and charcoal surfaces. The influence of cation valency is not as straightforward. For charcoal, larger q_{eq} in $CaCl_2$ than in NaCl solution was consistently observed in the whole range of c_{eq}'s. For soot, however, the q_{eq} was highest in $CaCl_2$ solution below c_{eq}~400 μgml^{-1} but above c_{eq}~450 μgml^{-1}, q_{eq} was comparable or even lower in $CaCl_2$ than in NaCl solution. DNA adsorbed at soot and charcoal even in pure water although with the lowest q_{eq} measured. The occurrence of adsorption in pure water, *i.e.* in absence of charge screening cations again suggest that electrostatic interaction is not the only one governing the adsorption.

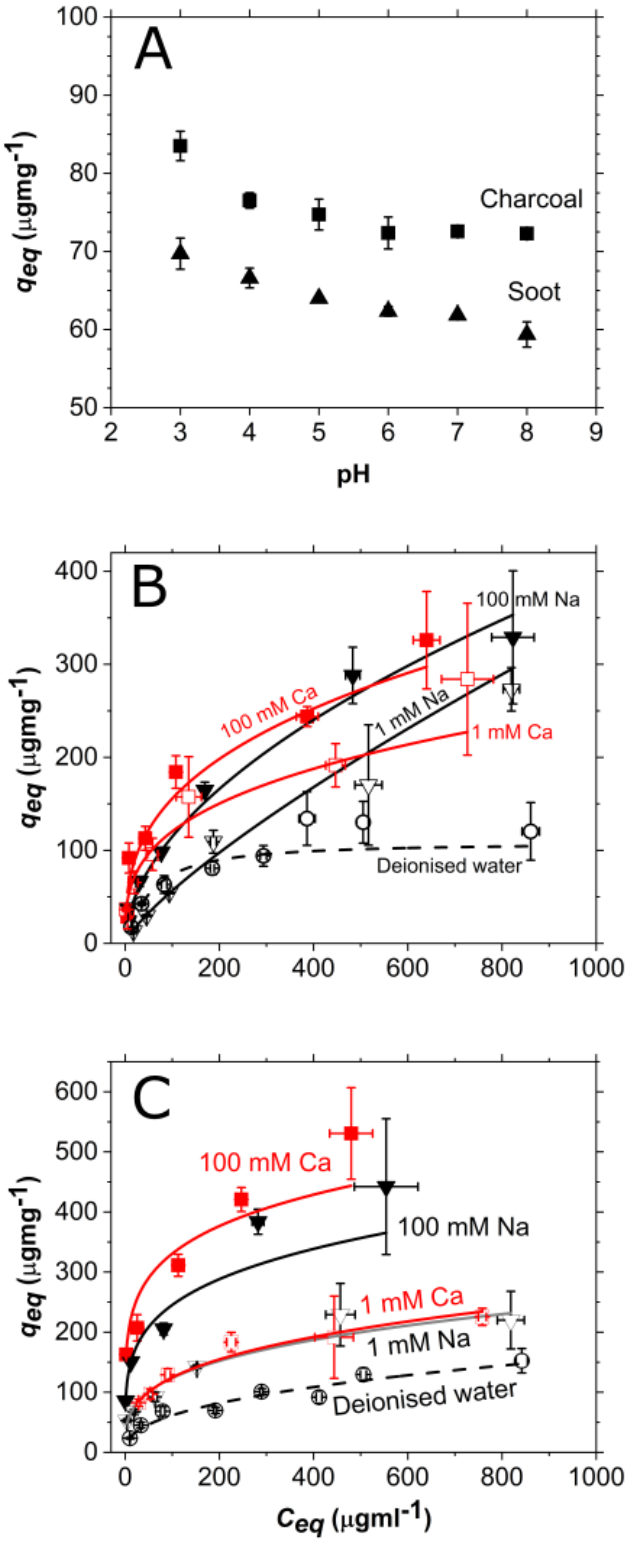

291

292 Figure 2. a) DNA adsorption capacity decreases as pH increases in solution with 100 mM NaCl and
293 with initial DNA concentration of 50 µgml^{-1}. Adsorption isotherms for b) soot and c) charcoal.
294 Experimental data are represented with symbols and best fits with lines (Freundlich model except
295 for soot in 1 mM $CaCl_2$ solution and deionised water that was best fit with the Sips model). All
296 uncertainties given as standard deviation.

To quantitatively describe the measured sorption relationships, we fit a range of models (Table S1) to the adsorption isotherms (Figure 2B-C, full lines). Based on χ^2_ν parameter, the best fit was to the Freundlich model, except for DNA adsorption at soot in pure water and 1 mM $CaCl_2$: in these cases, the data was best described with the Sips model (Table S3 and S4). The fit to the Freundlich model suggests that the DNA adsorption is a multilayer process[47] and that the surfaces are energetically heterogeneous, *i.e.* the surface sites at which the adsorption occurs are not of the same energy and abundance. At charcoal, the Freundlich constant, K_F, and the exponent, n, are lowest for adsorption in pure water (Table S3) suggesting that both the adsorption affinity towards DNA (estimated with K_F)[48] and the heterogeneity of the surface (estimated with n)[48] are lowest when there are no cations in solution. The dependence between K_F and n, and cation concentration and valency is expected since both the surface heterogeneity of a material and the surface charge density vary as a function of ionic strength, which influences the surface potential.[49] The surface affinity towards DNA and the charcoal surface heterogeneity in the presence of 1 mM is significantly lower than in the presence of 100 mM of either Na^+ or Ca^{2+}. Thus, the DNA adsorption capacity at charcoal follows the trend (Table S3):

$$q_{eq}\text{ (DNA, charcoal)} \rightarrow \text{pure water} < 1\text{ mM NaCl} \sim 1\text{ mM } CaCl_2 < 100\text{ mM NaCl} < 100\text{ mM } CaCl_2. \quad \text{Eq 4}$$

We observed a similar trend for adsorption at soot that was best described with the Freundlich model (Table S3):

$$q_{eq}\text{ (DNA, soot)} \rightarrow 1\text{ mM NaCl} < 100\text{ mM NaCl} < 100\text{ mM } CaCl_2. \quad \text{Eq 5}$$

In contrast, the better fit of isotherms at soot in pure water and 1 mM $CaCl_2$ to the Sips model suggests that the surface is still best described as energetically heterogeneous although DNA adsorption has theoretically happens as monolayer,[50] *i.e.* there exists a maximum adsorption capacity (q_{max}) (Table S3). q_{max}, and in fact q_{eq} at each c_{eq}, at soot in 1 mM $CaCl_2$ solution is ~3.5x higher than in pure water, *i.e.*:

$$q_{eq}\text{ (DNA, soot)} \rightarrow \text{pure water} < 1\text{ mM } CaCl_2. \quad \text{Eq 6}$$

A ramification of the Sips equation is that when n_s=1, the model reduces to the Langmuir equation (Table S1) implying that the surface is homogeneous, *i.e.* there is only one type of adsorption site. The n_s=1.16 for adsorption at soot in pure water suggesting that DNA adsorbs at few adsorption sites. This is also corroborated with good fits of the isotherm obtained in pure water to the Langmuir model (Table S4). However, n_s=0.42 for adsorption in 1 mM $CaCl_2$ suggesting that the surface is heterogeneous with many adsorption sites. We conclude that, for soot, the surface heterogeneity in electrolyte solutions is a consequence of strong ion binding and formation of new sites. In contrast, charcoal contains many active sites for DNA adsorption already in pure water and gains more with strong ion binding as solution concentration increases.

Adsorption kinetics. To obtain a more comprehensive insight into the mechanism of DNA adsorption at charcoal and soot, we measured the concentration of adsorbed DNA, q_t, as a function of time, t, at 283 K, 293 K and 303 K (Figure 3A-B). q_t started plateauing at ~300 min suggesting that the equilibrium was reached. We continued to monitor the q_t for another 24 h to obtain a reliable estimates of q_t at infinite time, q_∞.

Adsorption of DNA at soot and charcoal happens quickly. For soot, half of the DNA adsorbed in <1 min at 303 K, ~1 min at 293 K and ~3 min at 283 K (Figure 3A). For charcoal, the adsorption was slower: ~1

min at 303 K, ~2 min at 293 K and ~4 min at 283 K (Figure 3B). After 360 min, both soot and charcoal adsorbed majority of the DNA.

To quantitatively assess these observations, we fit the kinetic data to various adsorption kinetic models (Table S1). The best fit was achieved with the Ritchie 3rd order kinetic model (Table S4). This, however, suggests that the adsorption is not diffusion- but surface-controlled, *i.e.* the mass transfer depends only on the rate of DNA adsorption on active surface sites and not the rate of its transfer through the solution to the particle.

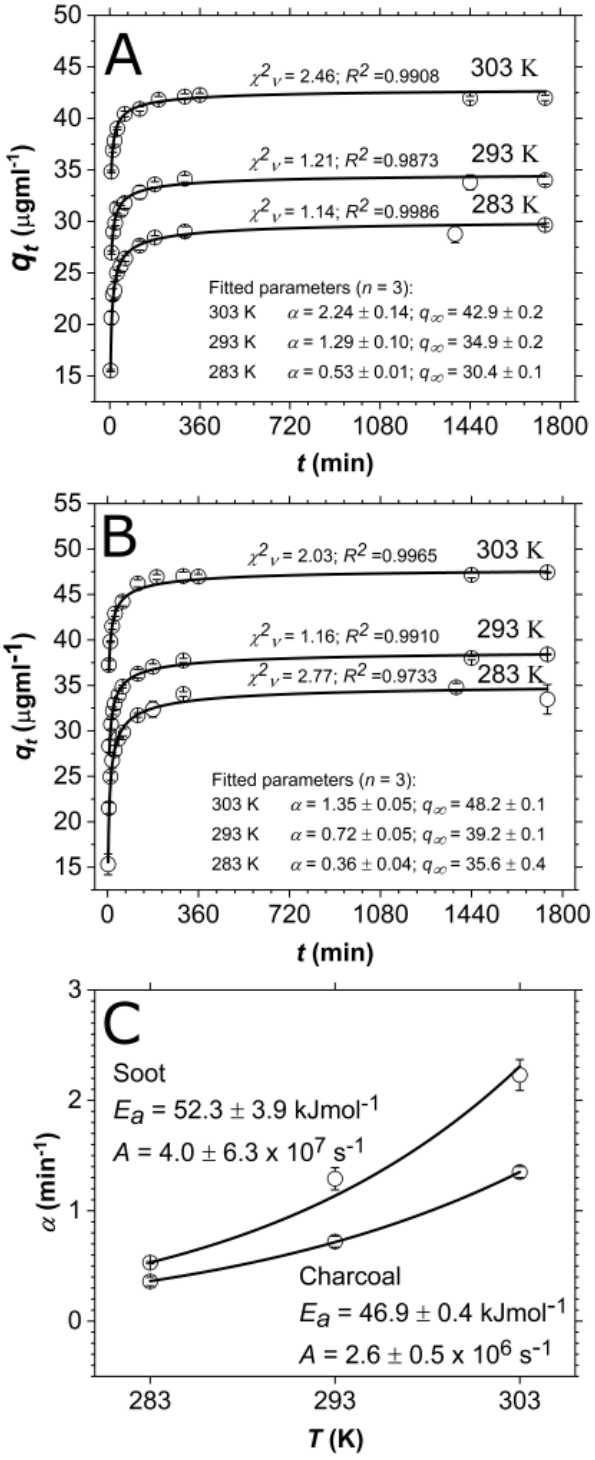

Figure 3. Kinetic experimental data (empty circle) with the Ritchie kinetic model (full line), corresponding quality of fits (χ^2_ν, R^2) and fitted parameters for a) soot and b) charcoal. q_∞ expressed in μgml^{-1} and α in min^{-1}. Adsorption conducted in 100 mM NaCl and pH=7. c) Arrhenius plot derived from the kinetic rates (empty circle) showing a logarithmic fit to the data (full line) with the calculated adsorption activation energy (E_a) and the kinetic pre-factor (A). All uncertainties given as standard deviation.

To estimate the activation energy, E_a, required for adsorption of DNA at soot and charcoal, we plotted α as a function of temperature, T (Figure 3C). We calculated E_a by fitting the plot to the Arrhenius equation:[51]

$$\alpha = Ae^{\frac{E_a}{RT}}, \qquad \text{Eq 7}$$

where A represents kinetic pre-factor (min^{-1}), and R the gas constant (8.3145 J mol^{-1}K^{-1}). We observed that somewhat higher energy is required to adsorb DNA at soot (E_a=52.3 ± 3.9 kJmol^{-1}) than at charcoal (E_a=46.9 ± 0.4 kJmol^{-1}) suggesting that interaction between DNA and soot is stronger than DNA and charcoal. Given the heterogeneous nature of the active sites at soot and charcoal, the E_a's calculated using the Arrhenius equation are an average of likely many E_a's governing DNA adsorption. Regardless, the E_a's are >40 kJmol^{-1}, a rule of thumb value for differentiation between a physisorption and chemisorption, indicating a strong, perhaps a covalent interaction between DNA, and soot and charcoal.

Adsorption of long DNA. In soils, the length of DNA influences the q_{eq}[52,53] and likely the overall adsorption mechanism. To explore the role of DNA length on adsorption to CMs, we collected adsorption isotherms using <2000 kb DNA (long DNA) in 100 mM NaCl and in pure water (Figure 4A). Because of charge screening of DNA within the ion atmosphere,[54,55] the DNA in 100 mM NaCl is more coiled compared to DNA in water. Since supercoiled DNA adsorbs less to sand particles compared to linear or circular DNA,[3] the change in conformation cannot alone explain higher q_{eq} in 100 mM NaCl compared to water. Similarly to q_{eq} for ~30 kb DNA (short DNA) (Figure 2B-C), q_{eq} for long DNA at charcoal is larger than at soot in 100 mM NaCl. However, this is not the case in pure water where q_{eq} is higher at soot than at charcoal. This is the only instance where adsorption at soot was higher than at charcoal (Fig. 2B-C, Table S3). These observations can be explained by enhanced hydrophobic interactions in pure water compared to electrolytes where charges give rise to electrostatic attractive interaction.

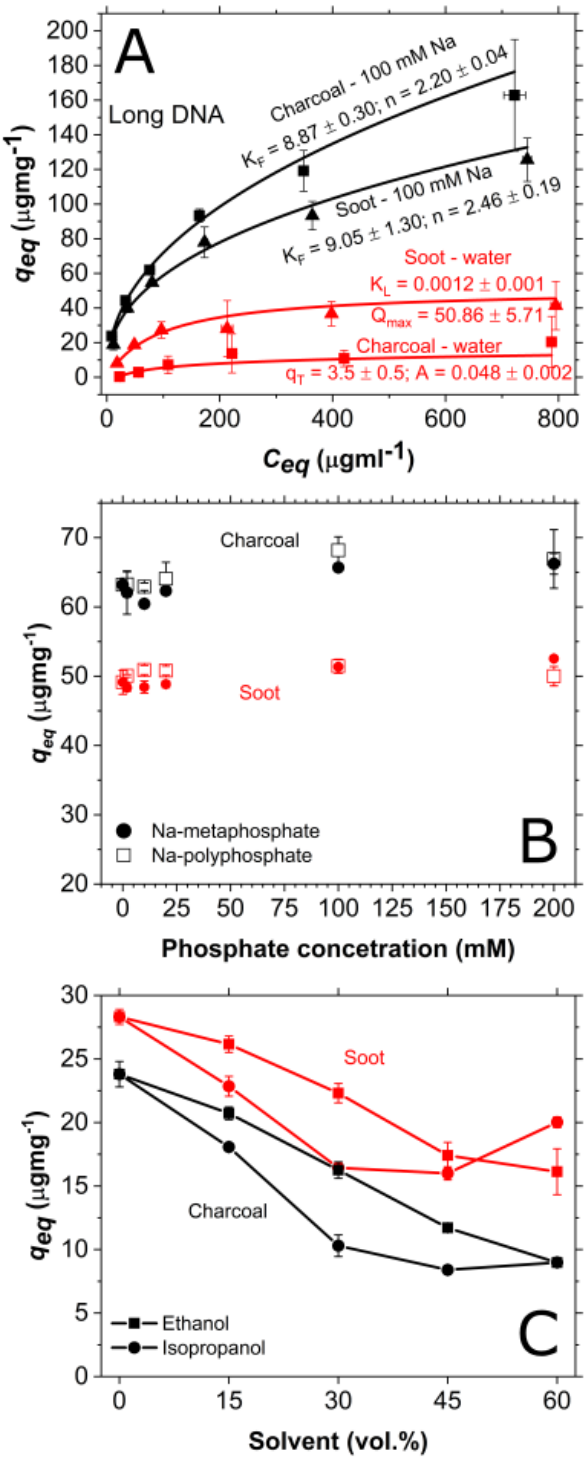

Figure 4. A) Adsorption data (symbols) of <2000 bp salmon sperm DNA and the corresponding isotherm models (lines). The capacity for long DNA is lower than for short DNA. There is a significantly larger difference in the adsorption capacity of DNA in pure water and 100 mM NaCl at charcoal than at soot suggesting that different interaction forces control adsorption of DNA at those two materials. K_F=Freundlich constant, K_L=Langmuir constant, Q_{max}=maximum adsorption capacity, q_T=Temkin capacity, A=Temkin isotherm constant (units in Table S1). B) q_{eq} does not significantly vary as a function of concentration of Na-polyphosphate and Na-metaphosphate suggesting that phosphate backbone of DNA does not play a significant role in adsorption to soot and charcoal. Initial DNA concentration ~50 µgml^{-1} (100 mM NaCl). C) c_{eq} of DNA decreases as the alcohol

concentration in the solution increases suggesting hydrophobic interaction plays a role in the DNA sorption to both materials. Initial DNA concentration was 50 $\mu g ml^{-1}$. Full lines are not the fit, and only serve as a guide to the eye. All uncertainties expressed as standard deviation.

The fitting to isotherm models revealed very similar behaviour as for the short DNA: The adsorption of long DNA in electrolytes is best describedby a multilayer adsorption model for anenergetically heterogeneous surface (quality of fit parameters in Table S6, model fits in Figure 4A). A better fit of the isotherm for charcoal in pure water to Temkin rather than Freundlich model suggest that there is either a uniform distribution of heterogeneous binding sites or that there is interaction between neighbouring DNA molecules.[56] Long DNA adsorption at soot in pure water is still best describedby a monolayer adsorption model(Langmuir model). This stands in contrast to adsorption of short DNA that is best described by model for monolayer adsorption at heterogeneous surface (Sips model, Table S3).

For long DNA, many of the tested models often fit the data well. Some fits had χ^2_ν very close to 1 but the value of standard deviation was larger than the fitted model parameters (red in Table S6). In these cases, we considered as the best, the fit that had χ^2_ν next in line but had standard deviation smaller than the fitted model parameters. The fact that the fitting parameters do not give a conclusive picture about the adsorption of long DNA suggests that the adsorption process is likely more complicated than in the case of short DNA. However, we did observe that all models that closely fit experimental data had similar assumptions and implications, *i.e.* adsorption of long DNA at soot in pure water is similarly well fit with both Langmuir and Toth models (Table S6). Since the *z* parameter of Toth model was ~1, this suggests that the adsorption is best described by a model for monolayer process but suggesting that the surface is heterogeneous.

Long DNA showed lower q_{eq} than short DNA both in 100 mM NaCl and pure water. This is a result of either enhanced steric hindrances as a consequence of size and charge variations of DNA or diffusion limited mass transfer of long DNA.[52,57] If steric hindrances increase with size, that would suggest that the phosphate backbone of DNA is responsible for interaction with soot and charcoal surfaces. To test this, we adsorbed short DNA in presence of polyphosphate and metaphosphate (Figure 4B) that compete with DNA for adsorption sites at negatively charged surfaces such as clay minerals.[53,58] We did not observe any changes in q_{eq} of DNA for a wide range of phosphate concentrations (0-200 mM PO_4^{3-} equivalent) suggesting that phosphate backbone is not responsible for DNA interaction with soot and charcoal, as observed on graphene materials.[29] Since the steric repulsion cannot account for lower q_{eq} of long compared to short DNA, the alternative explanation by which the adsorption is diffusion limited implies that a different mechanism controls adsorption of long and short DNA.

Hydrophobic interactions. To test our hypothesis that the hydrophobic forces play an important role in DNA adsorption at CM's, we measured the q_{eq} in mixtures of pure water and ethanol, and pure water and isopropanol (Figure 4C). These alcohols have lower dielectric constant than water (ε(water)=80, ε(ethanol)=25, ε(isopropanol)=18) so mixing them decreases the interfacial tension of water in contact with a hydrophobic surface, decreasing the hydrophobic interactions.[59,60] At ~40% of ethanol, the DNA conformation changes from a B-form predominant in aqueous solution to A-form.[61] The A-form is more compact than B-form and thus likely exhibits a higher charge density. If the electrostatic interaction controls the adsorption of DNA on soot and charcoal, the transition in conformation would suggest an increase in adsorption capacity as the alcohol concentration increases. However, if hydrophobic interactions influence adsorption, water-alcohol mixtures ought to retain DNA in solution because the entropic drive for partitioning DNA from the solution to the hydrophobic surface is diminished. We observed exactly that, a decrease in DNA adsorption when the volume fraction of either ethanol or isopropanol in the solution increased (Fig. 4C). In addition, a q_{eq} in

isopropanol was consistently lower than in ethanol solution, as expected since isopropanol is less polar than ethanol so there is a lower drive for DNA to escape it. An exception to this is a larger q_{eq} at 60 vol.% where we likely observed DNA precipitation in isopropanol but not in ethanol since higher ionic strengths are needed for DNA precipitation in ethanol mixtures.[62] Such adsorption behaviour was also observed on graphene oxide,[29] which is significantly more hydrophilic than either soot or charcoal.

Since the bulk hydrophobicity of both CM's is similar, the higher q_{eq} at soot than charcoal in pure water is perhaps a consequence of a strong heterogeneous distribution of hydrophobic sites at soot. This heterogeneity at soot is likely reflected in a more complex modeling of DNA adsorption (eqs 5 and 6) compared to charcoal (eq 4).

CONCLUSION

Elucidating the role of environmentally common CMs such as soot and charcoal in adsorption and stabilization of eDNA is important for better understanding of its cycling in environment. This study showed that the adsorption of dsDNA at soot and charcoal in general follows trends observed at graphene and graphene oxide surfaces. The adsorption capacity of dsDNA increases as pH decreases and as ionic strength increases, and it is generally higher for solutions containing divalent compared to monovalent cations. Such behavior reveals that electrostatic interaction contributes to DNA-CM binding since both soot and charcoal, and DNA are negatively charged at circumneutral pH but become positive at lower pH. That the adsorption capacity is generally higher for solutions containing divalent compared to monovalent cations suggests that attraction is, to an extent, established by charge screening between negatively charged surfaces and DNA. As revealed by adsorption modeling, the shape of adsorption isotherms in solutions of different pH and composition was similar but different between short and long DNA suggesting that adsorption mainly depends on the length of the DNA molecule but less so on the composition of the surface or the solution. However, the distribution of hydrophobic areas on soot and charcoal surfaces determine the extent to which the hydrophobic interactions will take place. Both soot and charcoal are similarly hydrophobic as evidenced by their water adsorption behavior. However, the contribution of hydrophobic interaction at soot was much stronger suggesting that regions which interact hydrophobically with DNA are more suitably distributed to allow adsorption compared to the same regions at charcoal. The majority of dsDNA adsorbs within minutes at both CMs with the activation energy of ~50 $kJmol^{-1}$ suggesting a strong binding. DNA that is bound so strongly to a surface likely cannot be desorbed by common extraction techniques suggesting that a wealth of genomic and ecologic information might remain hidden in samples after the extraction. Our results imply that dsDNA binds to both CM's by terminal basepairs and we showed that both electrostatic and hydrophobic interactions are important contributors to adsorption. The contribution of one or another interaction depends likely on the relative proportion of graphitic (hydrophobic) surfaces and those populated by oxygen functional groups. Combined, this study provides a fundamental understanding of dsDNA-CM interactions that can be used for improving DNA extraction protocols from environmental matrices containing CM. Our study covers a fraction of complex environmental conditions while future studies can investigate the interaction between dsDNA and CM in presence of heavy metals or other cellular organic compounds such as proteins or lipids. Such investigations would contribute to the comprehensive understanding of cycling of eDNA bound to CM's and its use in biomonitoring.

Our results demonstrate that CM's are likely reservoirs of extracellular eDNA in urban aerosol and topsoil and environments under influence of wildfires. These reservoirs can potentially be used for monitoring of biodiversity, and invasive and endangered species.

ACKNOWLEDGMENTS

We thank Enrico Cappellini for access to Biophotometer. KKS and SJ are grateful for a research grant from VILLUM FONDEN (00025352). SJ was partly funded by French Government through MOPGA

Postdoctoral Programme (reference number 3—5402234721). The geochemistry-mineralogy platform of ISTerre (Grenoble, France) is partially funded by a grant from Labex OSUG@2020 (investissements d'avenir, ANR10-LABX56). SM was funded by the VILLUM FONDEN (Grant numbers 00022942).

CONFLICTS OF INTEREST

Authors declare no conflicts of interest.

REFERENCES:

1. Slon, V. *et al.* Neandertal and Denisovan DNA from Pleistocene sediments. *Science* **356**, 605–608 (2017).
2. Pedersen, M. W. *et al.* Environmental genomics of Late Pleistocene black bears and giant short-faced bears. *Current Biology* **31**, 2728-2736.e8 (2021).
3. Romanowski, G., Lorenz, M. G. & Wackernagel, W. Adsorption of plasmid DNA to mineral surfaces and protection against DNase I. *Appl. Environ. Microbiol.* **57**, 1057–1061 (1991).
4. Paget, E., Monrozier, L. J. & Simonet, P. Adsorption of DNA on clay minerals: protection against DNaseI and influence on gene transfer. *FEMS Microbiology Letters* **97**, 31–39 (1992).
5. Khanna, M. & Stotzky, G. Transformation of Bacillus subtilis by DNA bound on montmorillonite and effect of DNase on the transforming ability of bound DNA. *Appl Environ Microbiol* **58**, 1930–1939 (1992).
6. Thomsen, P. F. & Willerslev, E. Environmental DNA – An emerging tool in conservation for monitoring past and present biodiversity. *Biological Conservation* **183**, 4–18 (2015).
7. Bohmann, K. *et al.* Environmental DNA for wildlife biology and biodiversity monitoring. *Trends in Ecology & Evolution* **29**, 358–367 (2014).
8. Pedersen, M. W. *et al.* Ancient and modern environmental DNA. *Philosophical Transactions of the Royal Society B: Biological Sciences* **370**, 20130383 (2015).
9. Taberlet, P., Bonin, A., Zinger, L. & Coissac, E. *Environmental DNA: For Biodiversity Research and Monitoring*. (Oxford University Press, 2018). doi:10.1093/oso/9780198767220.001.0001.
10. Clare, E. L. *et al.* Measuring biodiversity from DNA in the air. *Current Biology* **32**, 693-700.e5 (2022).

11. Lynggaard, C. *et al.* Airborne environmental DNA for terrestrial vertebrate community monitoring. *Current Biology* **32**, 701-707.e5 (2022).
12. Schmidt, M. W. I. & Noack, A. G. Black carbon in soils and sediments: Analysis, distribution, implications, and current challenges. *Global Biogeochemical Cycles* **14**, 777–793 (2000).
13. Xi, J., Yang, G., Cai, J. & Gu, Z. A Review of Recent Research Results on Soot: The Formation of a Kind of Carbon-Based Material in Flames. *Frontiers in Materials* **8**, 179 (2021).
14. Franklin, R. E. & Randall, J. T. Crystallite growth in graphitizing and non-graphitizing carbons. *Proceedings of the Royal Society of London. Series A. Mathematical and Physical Sciences* **209**, 196–218 (1951).
15. Sadezky, A., Muckenhuber, H., Grothe, H., Niessner, R. & Pöschl, U. Raman microspectroscopy of soot and related carbonaceous materials: Spectral analysis and structural information. *Carbon* **43**, 1731–1742 (2005).
16. Müller, J.-O., Su, D. S., Wild, U. & Schlögl, R. Bulk and surface structural investigations of diesel engine soot and carbon black. *Phys. Chem. Chem. Phys.* **9**, 4018–4025 (2007).
17. Pyle, L. A. *et al.* Chemical and Isotopic Thresholds in Charring: Implications for the Interpretation of Charcoal Mass and Isotopic Data. *Environ. Sci. Technol.* **49**, 14057–14064 (2015).
18. Lindahl, T. & Andersson, A. Rate of chain breakage at apurinic sites in double-stranded deoxyribonucleic acid. *Biochemistry* **11**, 3618–3623 (1972).
19. Frederico, L. A., Kunkel, T. A. & Shaw, B. R. A sensitive genetic assay for the detection of cytosine deamination: determination of rate constants and the activation energy. *Biochemistry* **29**, 2532–2537 (1990).
20. Impellizzeri, K. J., Anderson, B. & Burgers, P. M. The spectrum of spontaneous mutations in a Saccharomyces cerevisiae uracil-DNA-glycosylase mutant limits the function of this enzyme to cytosine deamination repair. *J Bacteriol* **173**, 6807–6810 (1991).
21. Torti, A., Lever, M. A. & Jørgensen, B. B. Origin, dynamics, and implications of extracellular DNA pools in marine sediments. *Marine Genomics* **24**, 185–196 (2015).

528 22. Szabó, T. *et al.* Evolution of Surface Functional Groups in a Series of Progressively Oxidized
529 Graphite Oxides. *Chem. Mater.* **18**, 2740–2749 (2006).
530 23. Knauer, M. *et al.* Soot Structure and Reactivity Analysis by Raman Microspectroscopy,
531 Temperature-Programmed Oxidation, and High-Resolution Transmission Electron Microscopy. *J.*
532 *Phys. Chem. A* **113**, 13871–13880 (2009).
533 24. Erickson, K. *et al.* Determination of the Local Chemical Structure of Graphene Oxide and
534 Reduced Graphene Oxide. *Advanced Materials* **22**, 4467–4472 (2010).
535 25. Zhao, X. Self-Assembly of DNA Segments on Graphene and Carbon Nanotube Arrays in
536 Aqueous Solution: A Molecular Simulation Study. *J. Phys. Chem. C* **115**, 6181–6189 (2011).
537 26. He, S. *et al.* A Graphene Nanoprobe for Rapid, Sensitive, and Multicolor Fluorescent DNA
538 Analysis. *Advanced Functional Materials* **20**, 453–459 (2010).
539 27. Lei, H. *et al.* Adsorption of double-stranded DNA to graphene oxide preventing enzymatic
540 digestion. *Nanoscale* **3**, 3888–3892 (2011).
541 28. Tang, L., Chang, H., Liu, Y. & Li, J. Duplex DNA/Graphene Oxide Biointerface: From
542 Fundamental Understanding to Specific Enzymatic Effects. *Advanced Functional Materials* **22**,
543 3083–3088 (2012).
544 29. Wu, M., Kempaiah, R., Huang, P.-J. J., Maheshwari, V. & Liu, J. Adsorption and Desorption of
545 DNA on Graphene Oxide Studied by Fluorescently Labeled Oligonucleotides. *Langmuir* **27**, 2731–
546 2738 (2011).
547 30. Huang, P.-J. J. & Liu, J. Molecular Beacon Lighting up on Graphene Oxide. *Anal. Chem.* **84**,
548 4192–4198 (2012).
549 31. Liu, Z. *et al.* Direct observation of oxygen configuration on individual graphene oxide sheets.
550 *Carbon* **127**, 141–148 (2018).
551 32. Liu, Z., Rios-Carvajal, T., Ceccato, M. & Hassenkam, T. Nanoscale chemical mapping of
552 oxygen functional groups on graphene oxide using atomic force microscopy-coupled infrared
553 spectroscopy. *Journal of Colloid and Interface Science* **556**, 458–465 (2019).

554 33. Tuinstra, F. & Koenig, J. L. Raman Spectrum of Graphite. *J. Chem. Phys.* **53**, 1126–1130
555 (1970).
556 34. Beny-Bassez, C. & Rouzaud, J. N. Characterization of Carbonaceous Materials by Correlated
557 Electron and Optical Microscopy and Raman Microspectroscopy. *Scanning Electron Microscopy*
558 119–132 (1985).
559 35. Wang, Y., Alsmeyer, D. C. & McCreery, R. L. Raman spectroscopy of carbon materials:
560 structural basis of observed spectra. *Chem. Mater.* **2**, 557–563 (1990).
561 36. Sze, S.-K., Siddique, N., Sloan, J. J. & Escribano, R. Raman spectroscopic characterization of
562 carbonaceous aerosols. *Atmospheric Environment* **35**, 561–568 (2001).
563 37. Beyssac, O., Goffé, B., Chopin, C. & Rouzaud, J. N. Raman spectra of carbonaceous material
564 in metasediments: A new geothermometer. *Journal of Metamorphic Geology* **20**, 859–871 (2002).
565 38. Ŝalac, S. & Kallay, N. Application of mass titration to the point of zero charge determination.
566 *Journal of Colloid and Interface Science* **149**, 233–240 (1992).
567 39. Preočanin, T. & Kallay, N. Application of »Mass Titration« to Determination of Surface
568 Charge of Metal Oxides. *Croatica Chemica Acta* **71**, 1117–1125 (1998).
569 40. Saeki, K., Kunito, T. & Sakai, M. Effect of Tris-HCl Buffer on DNA Adsorption by a Variety of
570 Soil Constituents. *Microbes and Environments* **26**, 88–91 (2011).
571 41. Noh, J. S. & Schwarz, J. A. Estimation of surface ionization constants for amphoteric solids.
572 *Journal of Colloid and Interface Science* **139**, 139–148 (1990).
573 42. Bandosz, T. J., Jagiello, Jacek. & Schwarz, J. A. Comparison of methods to assess surface
574 acidic groups on activated carbons. *Anal. Chem.* **64**, 891–895 (1992).
575 43. Menéndez, J. A., Illán-Gómez, M. J., y León, C. A. L. & Radovic, L. R. On the difference
576 between the isoelectric point and the point of zero charge of carbons. *Carbon* **33**, 1655–1657
577 (1995).

578 44. Karanfil, T. & Kilduff, J. E. Role of Granular Activated Carbon Surface Chemistry on the
579 Adsorption of Organic Compounds. 1. Priority Pollutants. *Environ. Sci. Technol.* **33**, 3217–3224
580 (1999).
581 45. Popovicheva, O. *et al.* Water interaction with hydrophobic and hydrophilic soot particles.
582 *Phys. Chem. Chem. Phys.* **10**, 2332–2344 (2008).
583 46. Liu, L. *et al.* Water adsorption on carbon - A review. *Advances in Colloid and Interface Science*
584 **250**, 64–78 (2017).
585 47. Freundlich, H. Über die Adsorption in Lösungen. *Zeitschrift für Physikalische Chemie* **57U**,
586 385–470 (1907).
587 48. Schwarzenbach, R. P., Gschwend, P. M. & Imboden, D. M. *Environmental Organic Chemistry*.
588 (John Wiley & Sons, 2016).
589 49. Grahame, D. C. Diffuse Double Layer Theory for Electrolytes of Unsymmetrical Valence
590 Types. *J. Chem. Phys.* **21**, 1054–1060 (1953).
591 50. Sips, R. On the Structure of a Catalyst Surface. *J. Chem. Phys.* **16**, 490–495 (1948).
592 51. Arrhenius, S. Über die Reaktionsgeschwindigkeit bei der Inversion von Rohrzucker durch
593 Säuren. *Zeitschrift für Physikalische Chemie* **4U**, 226–248 (1889).
594 52. Ogram, A. V., Mathot, M. L., Harsh, J. B., Boyle, J. & Pettigrew, C. A. Effects of DNA Polymer
595 Length on Its Adsorption to Soils. *Appl Environ Microbiol* **60**, 393–396 (1994).
596 53. Pietramellara, G., Franchi, M., Gallori, E. & Nannipieri, P. Effect of molecular characteristics
597 of DNA on its adsorption and binding on homoionic montmorillonite and kaolinite. *Biol Fertil Soils*
598 **33**, 402–409 (2001).
599 54. Jacobson, D. R. & Saleh, O. A. Counting the ions surrounding nucleic acids. *Nucleic Acids*
600 *Research* **45**, 1596–1605 (2017).
601 55. Lipfert, J., Doniach, S., Das, R. & Herschlag, D. Understanding Nucleic Acid–Ion Interactions.
602 *Annual Review of Biochemistry* **83**, 813–841 (2014).

603 56. Pursell, C. J., Hartshorn, H., Ward, T., Chandler, B. D. & Boccuzzi, F. Application of the Temkin
604 Model to the Adsorption of CO on Gold. *J. Phys. Chem. C* **115**, 23880–23892 (2011).
605 57. Franchi, M. *et al.* Clay-Nucleic Acid Complexes: Characteristics and Implications for the
606 Preservation of Genetic Material in Primeval Habitats. *Orig Life Evol Biosph* **29**, 297–315 (1999).
607 58. Saeki, K., Kunito, T. & Sakai, M. Effects of pH, ionic strength, and solutes on DNA adsorption
608 by andosols. *Biol Fertil Soils* **46**, 531–535 (2010).
609 59. Yaacobi, M. & Ben-Naim, A. Hydrophobic interaction in water-ethanol mixtures. *J Solution*
610 *Chem* **2**, 425–443 (1973).
611 60. Ballal, D. & Chapman, W. G. Hydrophobic and hydrophilic interactions in aqueous mixtures
612 of alcohols at a hydrophobic surface. *J. Chem. Phys.* **139**, 114706 (2013).
613 61. Marchetti, S., Onori, G. & Cametti, C. Ethanol-induced compaction of DNA: a viscosimetry
614 and dynamic light scattering study. *Philosophical Magazine* **87**, 525–534 (2007).
615 62. Herskovits, T. T. Nonaqueous solutions of DNA: Factors determining the stability of the
616 helical configuration in solution. *Archives of Biochemistry and Biophysics* **97**, 474–484 (1962).
617